European Polymer Journal 210 (2024) 112967

Contents lists available at ScienceDirect

European Polymer Journal

journal homepage: www.elsevier.com/locate/europolj

From cocoa waste to sustainable bioink: valorising pectin for circular economy-driven tissue engineering

Joel Girón-Hernández [a,*], Abraham Tombe [b], Mufeeda Chemban Koyilot [b], Karen T. Salas-Calderón [c], Alex Charlton [d], Corinne Wills [d], Piergiorgio Gentile [b,*]

[a] Department of Applied Sciences, Faculty of Health and Life Sciences, Northumbria University, NE1 8ST Newcastle Upon Tyne, the United Kingdom of Great Britain and Northern Ireland
[b] School of Engineering, Newcastle University, NE1 7RU Newcastle Upon Tyne, the United Kingdom of Great Britain and Northern Ireland
[c] Centro Surcolombiano de Investigación en Café, Universidad Surcolombiana, 410010 Neiva, Colombia
[d] School of Natural and Environmental Sciences, Newcastle University, NE1 7RU Newcastle upon Tyne, the United Kingdom of Great Britain and Northern Ireland

ARTICLE INFO

Keywords:
Pectin
Cocoa pod husk waste
Bioink
Cartilage
Tissue engineering

ABSTRACT

Cocoa bean production, a cornerstone of many developing economies, currently adheres to a linear economic model, giving rise to sustainability concerns. The expansion of cocoa butter and liquor consumption has resulted in the increased generation of residual biomass, constituting 60–70 % of fresh fruit. The absence of management plans for this biomass in cocoa-producing countries poses a risk of phytosanitary issues. This study proposed a circular economy approach by valorising cocoa pod husk-derived pectin for tissue engineering. The study optimised an alkaline-based protocol to extract pectin from cocoa pod husk, resulting in ~ 20 % yield with a ~ 47 % degree of esterification. Methacrylation transformed extracted pectin into pectin methacrylate (PECMA), confirmed by FTIR-ATR and NMR analyses. PECMA hydrogels, crosslinked with $CaCO_3$ and UV, exhibited rapid gelation and superior water uptake properties. SEM revealed distinct morphological differences with UV exposure, showing improved interconnectivity and anisotropic porosity while the mechanical testing demonstrated enhanced compressive modulus and rheological properties with UV crosslinking. PECMA-based bioink encapsulated chondrocytes, maintaining cell viability over 6 days. This innovative bioink, derived from cocoa waste, holds promise for sustainable tissue engineering applications.

1. Introduction

The polymers derived from conventional petro-based materials play a significant role in advancing the quality of modern life. Nevertheless, the use of petro-based polymers is associated with certain inherent drawbacks, particularly concerning environmental pollution and end-of-life disposal options [1]. Therefore, raw materials derived from terrestrial and marine animals, agricultural plants, microorganisms, and their residues represent valid alternatives to the potrelum as the most biologically renewable resources. Indeed, these resources can be isolated and extracted from sustainable biomass materials, with agricultural plants, in particular, serving as a prominent source [2]. Among the most worldwide commodities, cocoa holds significant economic importance as a crop in developing nations. However, this brings a substantial amounts of underutilised by-products, such as cocoa bean shell and pod husk (CPH), produced during the extraction of beans from cocoa pods. Constituting approximately > 60–70 % of the entire fruit, CPH serves as the primary by-product of the processing [3]. Consequently, the adoption of by-product valorisation processes aligns with the principles of a circular economy, promoting the sustainability of the agricultural sector. [4].

Moreover, there have been few initiatives focusing explicitly on leveraging cocoa biowaste for extracting biomolecules and investigating their properties for potential biomedical applications, such as tissue engineering. Recently, pulverised cocoa bean shells, primarily composed of cellulose, lignin, and hemicellulose, have been suggested as reinforcements to improve the bioactivity and mechanical characteristics of polylactic acid filaments [5]. Additionally, Athanassiou et al. manufactured biofilaments composed of biodegradable polycaprolactone and micronised cocoa bean shell waste, successfully validating their utilisation in creating 3D printed specimens via Fused Deposition Modelling [6]. However, no studies in the literature have

* Corresponding authors.
E-mail addresses: joel.l.g.hernandez@northumbria.ac.uk (J. Girón-Hernández), piergiorgio.gentile@ncl.ac.uk (P. Gentile).

https://doi.org/10.1016/j.eurpolymj.2024.112967
Received 17 December 2023; Received in revised form 29 February 2024; Accepted 23 March 2024
Available online 24 March 2024

reported on the utilisation of cocoa pod husk biowaste, which is rich in biopolymers such as pectin and antioxidants, as a potential biomaterial for tissue engineering. In this scenario, pectin is one of the largest polysaccharides present on plant biomass, with high molecular weight that form polymers of D-galacturonic acid units linked by α-glycosidic bonds (1–4), with carboxyl groups that are partially esterified with methanol or ethanol. For the extraction of pectin, different methods have been reported in literature; among them the alkaline-based procedures have garnered attention due to the final characteristics of extracted pectin. For example, the preservation of neutral sugar side chains in the polysaccharide structure has been observed, resulting in a material with good ion binding capacity [7]. Moreover, a study conducted on grapefruit peel (*Citrus paradisi*) involved adjusting the pH of the extractant solution to 9, 10 and 11, using 6 M solution of NaOH at 80 °C for 1 h with continuous stirring, yielding approximately 21 % pectin extraction. This pectin possessed a rhamnogalacturonan I content of about 47 %, and exhibited a three-dimensional porous surface nanostructure, resulting in excellent ion-binding capacity for ions such as K^{+}, Ca^{2+}, and Fe^{3+} [8]. Additionally, the capacity of pectin to form gels under various conditions makes it valuable for technological applications. However, before exploring the gelation properties, it is crucial to understand its key feature, such as galacturonic acid content and degree of esterification (DE), that represents the proportion of esterified units in relation to their total galacturonic acid content. Based on DE, pectin is categorised as high methoxyl (DE $\geq$ 50 %) or low methoxyl (DE $<$ 50 %). Consequently, low methoxyl pectin can gel with divalent cations, while high methoxyl pectin gels under acidic pH and in the presence of high sugar concentrations [9].

Due to its physico-chemical properties, pectin has been proposed as potential component of ink formulation to be used in biopriting with the tissue engineering field [10]. A bioprinting ink, by definition, is a solution that can be aqueous, containing either a single biopolymer or a mixture of biopolymers with unique property of rapidly thickening or gelling upon extrusion. When living cells are incorporated as a component in the formulation of printing ink, it is commonly referred to as 'bioink' [11]. Developing a suitable printable bioink can be a challenging task, as it requires careful consideration of various chemical, physical, and biological factors, that include printability, printing reliability, biocompatibility, cell-instructive capabilities, rheological properties, mechanism of gelation, physical stability, and easy handling [12]. Furthermore, it is crucial to note that pectin has a structure that is remarkably alike to glycosaminoglycans (GAG) present in the ECM of human cartilage, representing an immense advantage in utilising pectin for tissue engineering [13].

When considering 3D printing using pectin-based inks, several crucial parameters must undergo thorough evaluation. These parameters encompass the esterification degree, the overall ink composition, the printing temperature, and the feasibility of chemically modifying the pectin structure to enhance specific attributes of the printed object. These enhancements could involve improving mechanical properties, enhancing cell adhesion characteristics, or optimising the crosslinking process. Literature reports different works where the pectin has been used in potentials blends with other polymer or additives like nanocellulose or sucrose [14]. For example, printing ink formulations utilising a combination of pectin and Pluronic® F-127 have been proposed due to the unique thermo-sensitive characteristic of Pluronic® F-127 that plays a pivotal role in this blended ink [15]. It remains in a liquid state at lower temperatures, facilitating smooth extrusion from the printing nozzle. However, when placed on a printing bed kept at 37 °C, the ink undergoes gelation. Nevertheless, it is important to note that structures created with pectin/Pluronic® F-127 inks often exhibit limited stability and may require additional crosslinking with calcium ions to enhance their structural integrity. Recently, 3D bioprinted hydrogels composed of Rhamnogalacturonan-I (RG-I) which is one of the domains of pectin, sodium alginate and gelatin have been successfully manufactured by Chang et al. [16]. It was observed that, among the various formulations tested, the bioink containing 500 μg/mL of pectin RG-I exhibited the most favorable characteristics, suggesting its potential suitability for repairing osteochondral defects. This is attributed to its anti-inflammatory properties and its ability to inhibit fibrosis. Furthermore, alongside pectin-based blends, such as those incorporating gelatin [17] or nanocellulose [14], semi-synthetic derivatives such as pectin methacrylate (PECMA) [18] and pectin norbornene [19], have found applications in 3D printing. These materials offer distinct advantages due to their ability to undergo photocrosslinking. This unique property provides several benefits, including enhanced resolution and precise control over the biochemical, mechanical, and biodegradable aspects of the printed substrates, ultimately allowing for the fine-tuning of the cellular microenvironment.

Therefore, the primary goal of this work was to propose an innovative bioink suitable for extrusion-based bioprinting technology and we hypothesised that pectin extracted from cocoa pod husk could be considered a sustainable biomaterial for cartilage tissue engineering. To achieve this, an in house optimised alkaline-based protocol was proposed to extract the pectin from cocoa biowaste and, then, methacrylated by readapting a procedure optmised by the authors [20]. We assessed the quality of the extracted pectin, in terms of sugar composition and yield, and the physico-chemical and mechanical properties of the resulting hydrogels, using calcium carbonate ($CaCO_3$) as crosslinker at different molarity in combination with the UV photo-crosslinking. Subsequently, the extracted pectin was assessed biologically by using chondrocytes derived from immortalised mesenchymal stem cells (MSCs-C) for its cytocompatibility and, then, the resulting PECMA-based hydrogel was used as potential bioink by encapsulating the MSCs-C cells.

2. Materials and methods

2.1. Materials and chemicals

The powder derived from cocoa pod husks was supplied by Universidad Surcolombiana (Neiva, Colombia). Glacial acetic acid (ACS reagent, ≥99.7 %), hydrochloric acid (ACS reagent, 37 %), ethanol 96 %, sodium chloride (ACS reagent, ≥99.0 %), methacrylic anhydride, Dulbecco's Phosphate Buffer Saline (PBS), trizma base, lithium phenyl 2,4,6-trimethylbenzoyl-phosphinate, sodium hydroxide (reagent grade, ≥98 %), and trifluoroacetic acid (TFA) were purchased from Fisher Scientific, UK. Meanwhile, 1-Phenyl-3-methyl-5-pyrazolone (PMP) was provided by Apollo Scientific, UK. The sugar standards (≥97 %), including galacturonic acid (GalA), glucuronic acid (GlcA), galactose (Gal), glucose (Glc), mannose (Man), xylose (Xyl), rhamnose (Rha), arabinose (Ara), and all other chemicals such as acetonitrile, methanol, ammonium bicarbonate, ammonium hydroxide, and formic acid, were purchased from Sigma-Aldrich, UK. Additionally, Nylon membrane Titan3 (0.45 μm) filters were obtained from Thermo Scientific, UK, and glass vials were sourced from Chromatography Direct, UK. Finally, non-stick baking paper was purchased from Sainsbury, UK. All distilled water (dH_2O) was filtered through the Milli-Q® Water Purification System (IQ 7005, Merck, UK).

2.2. Pectin extraction from cocoa biowaste

2.2.1. Cocoa biowaste processing and preparation

Healthy Cocoa fruits (40 kg) were harvested in Huila (Colombia) from cocoa producing farms, then washed with clean water. After removing the beans, cocoa pod husk was cut on slices of ~ 2 cm and let them sun dry until constant weight. Once dry, CPH was ground until powder (~200 μm) using an MultiDrive basic mill (IKA, Germany), and moisture content of the CPH powder was determined by oven drying to constant weight at 100 °C [21]. The powder was stored in plastic bag at room temperature until further analysis.

2.2.2. Alkaline extraction

The extraction process was conducted by adapting methodologies proposed by various authors [22,23] with some modifications. Cocoa pod husk powder was dissolved in a glass bottle containing a 0.05 M NaOH solution at concentration of 2 % w/v. The mixture was heated to 70 °C using an ultrasonic bath S30H (Elma, Germany) operating at 280 W-50/60 Hz for 100 min. Subsequently, cellulose and pectin separation were achieved using a centrifuge model 5810R (Eppendorf, Germany) at 3000 rpm for 60 mins. Afterward, the supernatant was collected and combined with 96 % ethanol at a ratio of 2:1 (v/v) and then stored at 4 °C for 24 h to precipitate the pectin. Following refrigeration, the mixture was centrifuged at 2000 rpm for 30 min to recover the pectin (in pellet form), which was then placed on non-stick baking paper and dried in an incubator model MIR-154 with forced air circulation (Panasonic, Japan) at 37 °C until a constant weight was achieved. Finally, the pectin flakes were collected and stored for further analyses.

2.3. PECMA hydrogels preparation

Methacrylated PECMA was synthesised by reacting the extracted pectin (PEC) from cocoa pods husk with methacrylic anhydride (MA). This process involved dissolving 1 % w/v of PEC in TRIS 1 M (Trizma base) at pH 8.5–9.0 for 30 min at 60 °C, followed by the addition of MA (8 % w/v) to the PEC solution. The reaction was maintained at 50 °C for 5 h, and the resulting PECMA formulation was purified through a 3-day dialysis process against dH_2O using a cellulose membrane with a molecular weight cut-off of 11–14 kDa. Subsequently, the dialysed PECMA was lyophilised for 48 h in a freeze-dryer (Alpha 1–2 LDplus, CHRIST, Germany).

For the preparation of the hydrogels, freeze-dried PECMA underwent UV sterilisation (254 nm) and was subsequently dissolved at a concentration of 4 % (w/v) in dH_2O. This dissolution process took place under continuous stirring at 50 °C and was carried out for 3 to 4 h, with the solution shielded from light. As demonstrated previously by Scalzone et al. [20], a dual crosslinking (ionic and UV) was used for the formation of the hydrogels. Specifically, to the dissolved PECMA solution, the photoinitiator lithium phenyl 2,4,6-trimethylbenzoyl-phosphinate (LAP) was added at a concentration of 0.1 % w/v, while different amounts of $CaCO_3$ solutions (1:1 v/v ratio respect with PECMA volume) were included to achieve different concentrations (10, 40 and 80 mM). For UV crosslinking, we used a handheld 6 Watt Ultraviolet Lamp (Cole-Parmer, UK), positioned 5 mm away from the top surface of the samples. During this stage, the pH was measured, and titration was performed to achieve a final pH of 7.

2.4. Characterisation methods

2.4.1. Fourier transform infrared spectroscopy (FTIR-ATR)

Infrared spectra were performed at room temperature (20 ± 0.5 °C) and dry atmosphere, on pectin flakes samples and after chemical conjugation with methacrylic anhydride for getting the PECMA, by using an Agilent Cary 630 FTIR spectrophotometer (Agilent, EEUU) with ATR sampling accessory. The spectrum was obtained from the average of five readings and recorded from 550 to 4000 cm^{-1} at a resolution of 4 cm^{-1} and 32 scans.

2.4.2. ^1H NMR measurement

The extracted pectin and PECMA samples were subjected to NMR spectroscopy analysis. Saturated samples were prepared in 0.7 mL of D_2O, and an internal reference, TMSP-d4 [3-(trimethylsilyl)-2,2,3,3-tetradeuteropropionic acid] from Sigma-Aldrich, UK, was added at 0.0 ppm. The ^1H NMR spectra were recorded at 80 °C using a Bruker Advance III HD 700 MHz NMR spectrometer equipped with a BBO probe. Each spectrum consisted of 128 scans and 32 K datapoints (transformed to 128 K). Baseline corrections were applied before integration. The methacrylation degree (MD) was determined by the ratio of methacrylate groups to the free amine groups in gelatin before the methacrylation reaction as described in literature [24].

2.4.3. Sugar composition analysis

The sugar content in the extracted pectin was determined using established protocols [25,26] in two sequential steps. In the first step, for the polysaccharide hydrolysis, 1 mg of pectin was meticulously weighed and placed in a sealed glass vial. Then, 1000 µl of dH_2O and 500 µl of concentrated trifluoroacetic acid were added to achieve a concentration of 4 M. After sealing the vial, the mixture was heated at 120 °C for 90 min with continuous stirring. Subsequently, the sample was allowed to cool to room temperature, and 200 µl of methanol was added. The sample was evaporated to dryness using nitrogen and a heating block set at 80 °C. This evaporation step was repeated three times to eliminate trifluoroacetic acid. Finally, the dried hydrolysed pectin was reconstituted in 1 mL of dH_2O. The second step involved the monosaccharide derivatisation using 1-Phenyl-3-Methyl-5-Pyrazolone (PMP), where 200 µl of the hydrolysed pectin solution was mixed with 80 µl of 0.3 M sodium hydroxide and 80 µl of PMP in methanol. The mixture was incubated at 80 °C for 60 min, then cooled to room temperature and neutralised by adding 80 µl of 0.3 M HCl. Finally, the sample was diluted to 1 mL by adding 400 µl of water. Any excess PMP was removed by partitioning with CH_2Cl_2 (3 × 1 mL), and phase separation was achieved in a vortex FB15012 TopMix (Fisher Scientific, UK) at 30,000 rpm for 30 s. All sugar standards were subjected to the same hydrolysis and derivatisation conditions as the samples. Prior to chromatographic analysis, all samples were filtered through 0.45 µm hydrophilic nylon syringe filters.

A Waters UPLC system, equipped with a photodiode-array detector and a single quadrupole mass spectrometric detector, was employed for the analysis of PMP-derivatives. Separation was conducted using an Acquity UPLC C18 column (50 × 2.1 mm, 1.7 µm) maintained at a temperature of 25 °C. The mobile phase comprised (A) 20 mM NH_4HCO_3/NH_4OH (pH 9.2) combined with MeCN 85:15 (v/v) and (B) pure MeCN. Elution of PMP-derivatives followed an isocratic gradient: 0–8 min (0–5 %), 8–12 min (5–10 %), 12–15 min (10–20 %), 15–16 min (20–0 %), 16–17 min. The flow rate was set at 0.3 mL min^{-1}, and 5 µl injections were made. Peak identification was confirmed through co-chromatography with authentic samples and by analysing molecular masses. ESI–MS with positive polarity was utilised over a mass range of 400–1000 *m/z*, employing a scan time of 200 ms, a capillary voltage of 0.8 kV, and a cone voltage of 30 V, while maintaining a gas temperature of 600 °C. Pseudo-molecular ions of the tagged pentoses were detected at 481 *m/z*, deoxy-hexoses at 495 *m/z*, hexoses at 511 *m/z*, and uronic acids at 525 *m/z*. Quantification was based on UV detection at 250 nm.

2.4.4. Degree of esterification

The degree of esterification (DE) of the extracted pectin samples was determined using Fourier Transform Infrared spectroscopy [27]. Approximately 20 mg of the sample was dissolved in 5 mL of dH_2O, and the pH of the solution was adjusted to ~ 5.5 using 0.3 M HCl. At this pH, which is higher than the pKa of polygalactouronic acids (3.38), all non-esterified carboxylic groups in the pectin solution exist as carboxylate ions [28]. Once dried, spectra were recorded from a flake of pectin. After processing, including baseline correction and applying second derivative analysis, the area of peaks in the regions of 1780–1720 cm^{-1} associated with esterified carboxylic groups (COOH) and 1640–1600 cm^{-1} associated with non-esterified COO^- were used to calculate the degree of esterification based on the following equation.

$$DE(\%) = \frac{Area\ of\ \mathrm{COOH}}{Area\ of\ \mathrm{COOH} + Area\ of\ \mathrm{COO^-}} x100 \quad (1)$$

2.4.5. PECMA gelation time

The gelation time of the hydrogels was determined at room temperature using the test tube inversion method [29]. To measure the

gelation time of PECMA solutions (1 mL), they were exposed to a UV lamp emitting light at 365 nm to initiate photo-polymerisation. The test was conducted on PECMA solutions containing the LAP and different $CaCO_3$ amounts under UV exposure. The flowability of the samples was observed every 15 s by tilting the vials, and the gelation time was recorded when the solution stopped flowing.

2.4.6. Water uptake kinetics

To investigate the water absorption capacity of the developed hydrogels, three freeze-dried samples were used for each composition. Individual lyophilised PECMA gels (with different contents of $CaCO_3$ with/without exposure to UV) with dimensions of 5 mm in diameter and 6 mm in height, were weighed and then placed in separate 5 mL bijou vials containing 3 mL of Dulbecco's phosphate-buffered saline (PBS). These vials were stored at 37 °C. At various time intervals (30 mins, 1, 3, 5, 8, 24, and 48 h of incubation), the hydrogels were removed from the solutions, and the surfaces of the gels were gently blotted with filter paper. Their current wet weight (W_t) was measured and compared to their initial wet weight (W_i). The water uptake (WU) was calculated using the following equation:

$$WU(\%) = \frac{W_t - W_i}{W_i} \times 100 \quad (2)$$

2.4.7. Morphological analysis

The morphology of the freeze-dried hydrogels was examined using a JEOL JSM-5600LV Scanning Electron Microscope. Samples were cut into small squares with dimensions of 2 mm in diameter and 1 mm in height. These squares were then affixed to aluminium stubs using carbon tape and coated with gold using a BIO-RAD Sputter Coater machine. Subsequently, they were analysed at a working distance of 6 mm, employing an operating voltage of 20 kV at different magnifications. The images were processed using ImageJ software to assess the distribution of pore diameters for each sample. For each sample type, three images were analysed, with 50 pores measured in each image. The pore sizes were averaged to determine a mean pore size, assuming that all pores were circular in shape.

2.4.8. Rheological evaluations

Rheological assessments were performed using the MCR302e stress-controlled rheometer (Anton Paar GmbH, Austria). This rheometer was equipped with a Taylor-Couette geometry involving concentric cylinder setup. The inner cylinder had a diameter of 16.662 mm, and the gap between the cylinders was set at 0.504 mm. More specifically, a shear stress ramp, spanning from 0.001 to 1000 Pa, was administered to both uncrosslinked and UV crosslinked PECMA material, and the yield point was identified as the point of intersection between two linear regressions representing the plateau region and the viscosity-drop region on the viscosity-shear stress diagrams, signifying the onset of material flow [30]. Rotational shear-viscosity measurements were conducted in flow mode, with shear rates ranging from 0.1 to 100 s^{-1} or until the highest attainable shear rate before material loss occurred from the plate–plate system. Finally, a frequency sweep test was conducted, covering a range of angular frequencies (ω) from 100 to 0.1 rad/s while maintaining a strain value of 1 % within the linear viscoelastic range. To ensure accuracy and consistency, these rheological tests were performed in triplicate. The temperature was carefully maintained at 21 °C throughout each test, achieved using a Peltier system as a control parameter.

2.4.9. Static mechanical compression tests

The UniVert Test Device (UV-200–01, CellScale, Canada), equipped with 10 N load cell, was employed for the evaluation of the prepared hydrogels via compression testing. These samples (n = 5) were pre-formed in 24-multiwell plates and had dimensions of approximately 16 mm in diameter and 20 mm in height. Compression tests were executed at a crosshead speed of 2.5 mm/min, with loading continuing until the point of fracture was achieved. The compressive modulus was determined by calculating the slope of the initial linear segment of the stress–strain curve (0–10 %).

2.4.10. Cell tests

2.4.10.1. Cell culture and seeding. The human TERT immortalised bone marrow stromal cell line was cultured and differentiated into chondrocytes (MSCs-C), as previously described [31]. In brief, the cells were cultured at 37 °C with 5 % CO_2 in DMEM/F12, supplemented with 10 % fetal bovine serum (FBS), 2 mM l-glutamine, and 1 % penicillin/streptomycin (P/S). Once they reached 80 % confluence, the cells were induced to differentiate into chondrocytes by exposing them to a mixture of chondrogenic factors. This mixture included serum-free DMEM with P/S, supplemented with 1 % ITS + 1, 10 ng/mL TGF-β3, 40 μg/mL l-proline, 100 nM dexamethasone, and 50 μg/mL l-ascorbic acid-2-phosphate. The differentiation process continued for 21 days. MSCs-C were subsequently cultured in DMEM/F12 with 10 % FBS and 1 % P/S and were used for experimentation (passage 15).

Extracted pectin from cocoa biowaste. For biocompatibility assessments, various PEC solutions were prepared at different concentrations (1, 2.5, 5, 10, 20, 30, and 40 mg/mL) in a 48-multiwell plate. This was accomplished by dissolving pectin powders in DMEM and subsequently sterilising the solutions through filtration using a 0.22 μm Millex GP PES membrane syringe-driven filter unit (Millipore, SLS, UK) with the aid of 5 mL plastic syringes. Suspensions containing 10,000 cells in DMEM were seeded in 48-well plates, respectively. These plates were used for the various biological tests after being treated with the different diluted PEC solutions, and they were incubated at 37 °C with 5 % CO_2.

PECMA. To allow the encapsulation of the cells into the bioink formulation, a 4 % w/v PECMA solution was prepared containing 0.1 % w/v of LAP photoinitiator. Then, the cell pellet was then homogenised using 2 mL of the PECMA solution (achieving a concentration of 2×10^6 cells/mL). Within a 24-multiwell plate, 250 μl of PECMA solution was poured gently in each well by using a micropipette, and then, 250 μl 80 mM $CaCO_3$ solution was added in each well to achieve a final 2 % w/v concentration of PECMA. The photocrosslinking was started by mounting the 365 nm UV light above the well plate for five mins. After photocrosslinking, 500 μl DMEM media was added into each well, and stored in the incubator for further analysis, with a change of media every two days.

2.4.10.2. Evaluation of cell viability, metabolic activity, and morphology. Cell viability was evaluated using Live/Dead staining (LIVE/DEAD® Cell Imaging Kit, Life Technologies, Thermo Scientific, US) after 48 h. Following the manufacturer's instructions, the samples were rinsed with phosphate-buffered saline (PBS, Sigma-Aldrich, UK) and stained with a 150 μl solution containing 4 μM Ethidium homodimer-1 and 2 μM calcein in PBS. After a 30-mins incubation at room temperature, cells were examined using an EVOS M5000 fluorescence microscope to detect calcein (excitation/emission 488 nm/515 nm) and Ethidium homodimer-1 (excitation/emission 570 nm/602 nm).

The Presto Blue assay was employed to assess the metabolic activity of cells seeded with various diluted PEC solutions in 96-multiwell plates after 48 h of cell seeding. A Filter-based FLUOstar® Omega multi-mode reader (FLUOstar® Omega, Germany) was utilised to measure fluorescence (excitation at 560 nm and emission at 590 nm) after 1.30 h of incubation with a 10 % aliquot of Presto Blue (Thermo Scientific, USA). The results were expressed as mean values ± standard deviation.

Furthermore, cell morphology was observed by staining the cell nuclei and cytoskeleton after different times of cell seeding. In summary, cells were fixed with a 4 % paraformaldehyde solution for 15 mins, followed by three PBS washing steps. Cells were then permeabilised using 0.1 % v/v Tween20® in PBS for five mins. Rhodamine-phalloidin was prepared with a 1:100 dilution of phalloidin-tetramethylrhodamine

B isothiocyanate (Sigma Aldrich, P1951) in 1 % v/v Tween20® in PBS for 30 mins, followed by three PBS washes. A drop of DAPI (VECTASHIELD®) antifade mounting media was added to each sample, covered with a glass slide, and then imaged using an EVOS M5000 fluorescence microscope.

2.4.11. Statistical analysis

Results were expressed as means ± standard deviations. Statistical analysis of the results was conducted using GraphPad Prism Software (version 8.4.1). A One-way ANOVA with repeated measurements was initially employed. Subsequently, a Tukey's post hoc test was performed to identify the primary factors responsible for data variability. The level of statistical significance was established as follows: * for $p < 0.05$, ** for $p < 0.01$ and *** for $p < 0.0001$.

3. Results

Physico-chemical characterisation of extracted pectin from cocoa bio-waste. A freshly harvested cacao fruit had an average weight of 926.8 ± 152.7 g. After removing the cacao beans from the pod husk, the fruit components exhibited the following fresh weights, along with their corresponding percentage per fruit: cocoa pod husk 747.1 ± 138.6 g (80.7 %), beans 155.1 ± 51.7 g (16.8 %), and funiculus 23.1 ± 6.9 g (2.5 %). Finally, the moisture content of the pod husk after the drying process was 85.69 ± 1.73 %, while the resulting cocoa pods husk powder showed a moisture content of 9.03 ± 0.19 %. After completing the alkaline extraction process, the retrieved pectin yield was 19.35 ± 0.59 %. Furthermore, regarding the sugar composition of the extracted, pectin shown in Fig. 1, the galacturonic acid was the most abundant monosaccharide. Additionally, the amount of side regions (~32 %), containing arabinose, rhamnose, and galactose, fell within the expected range of 20–35 %.

Finally, the alkaline extracted pectin presented a degree of esterification of 46.7 ± 3.1 %.

PECMA chemical characterisation. In Fig. 2**A**, FTIR-ATR spectra for PEC and PECMA are presented. In the PEC spectrum, prominent peaks include the C–H bend at 665 cm^{-1}, C-O stretching at around 1050–1000 cm^{-1}, the symmetric COO^- stretching at 1412 cm^{-1}, the asymmetric stretching at 1618 cm^{-1}, the stretching vibration (C = O) (associated with the methyl-esterification of the pectin) in the bands at 1743 cm^{-1}, the stretching vibration of aliphatic $–CH_2$ and $–CH_3$ groups at 2970–2880 cm^{-1}, and the O–H stretching at 3420 cm^{-1} [23]. Then to confirm the methacrylation process, the PECMA spectrum, in addition to the characteristic PEC peaks, showed those typical of the methacrylate group, such as the double bond (C = C) stretches at 1414 cm^{-1}, and the

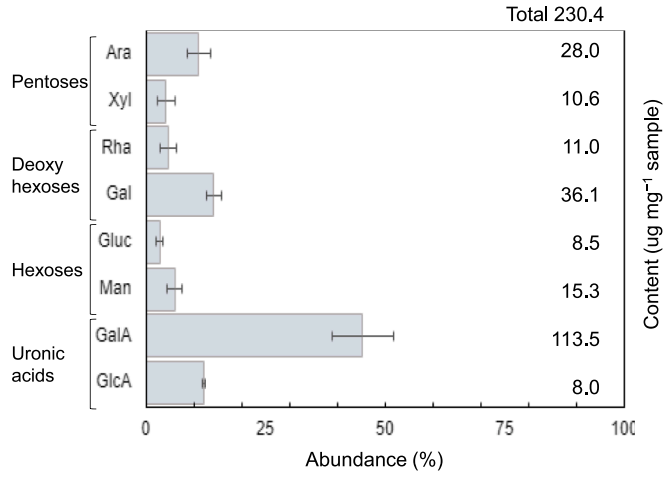

Fig. 1. Content (ug mg^{-1} sample) and abundance of sugar fractions quantified in the extracted pectin from CPH measured by UPLC.

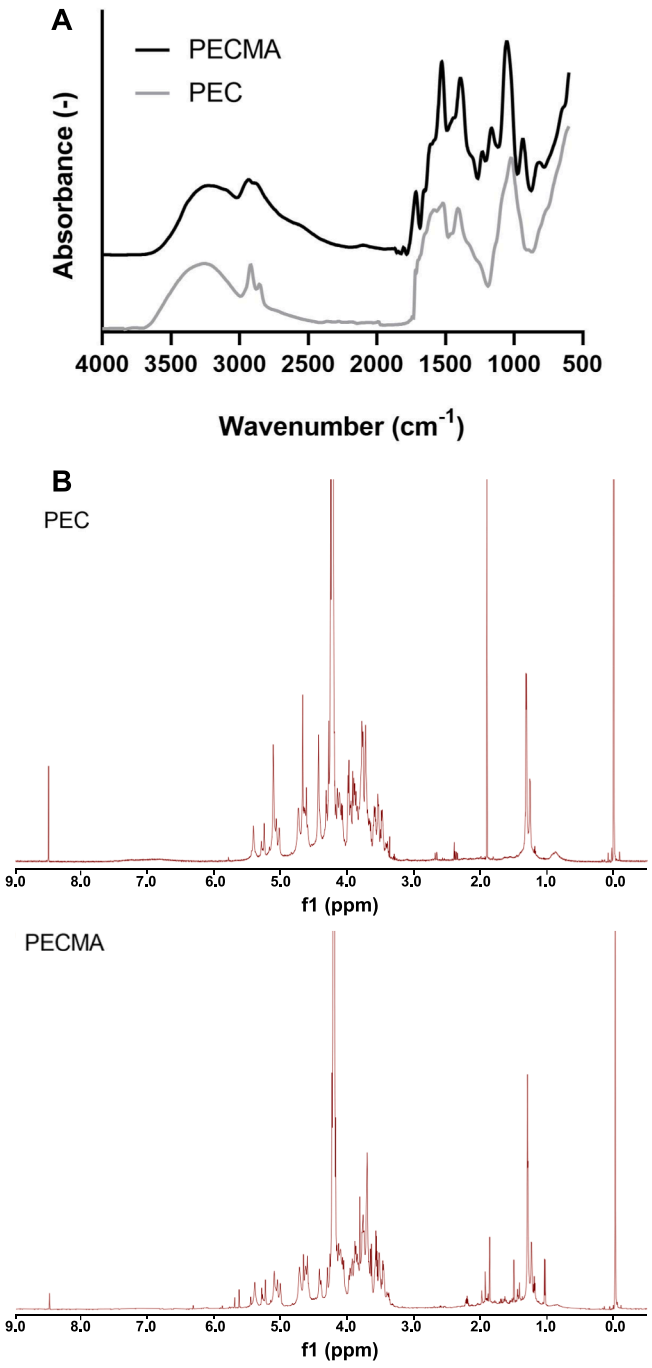

Fig. 2. FTIR-ATR (**A**) and NMR (**B**) spectra of pectin and methacrylated pectin.

peaks at 1530 and 1077 cm^{-1} related with C-N and C-O-C bonds [32]. Particularly, the C-N bonds are the backbone of PECMA as it is formed through the interaction of hydroxyl group (–OH) of the pectin with the anhydride group of the MA [33].

Additionally, the introduction of methacrylate groups into the PEC structure was confirmed by NMR analysis (Fig. 2**B**). In the chemical shift of unmodified PEC, distinctive signals appeared at 1.91 ppm originated from the $–COCH_3$ groups located at 3-O- and 2-O-galacturonic acid. Additionally, signals at 1.30 ppm and 1.27 ppm were attributed to the CH_3 group of L-rhamonose. The peak at 3.92 ppm corresponded to the CH_3 group associated with the carboxyl groups of GalA. The remaining pectin signals were assigned to the five protons in GalA (H_1, 5.05 ppm; H_2, 3.73 ppm; H_3, 3.97 ppm; H_4, 4.16 ppm, and H_5, 4.70 ppm). Furthermore, signal at 5.13 ppm identified as H_1 Rha. These

characteristic signals were also evident in the chemical shift for PECMA. Furthermore, the PECMA spectra exhibited new singlets at 1.96, 5.77, and 6.18 ppm, attributed respectively to the methyl proton of methacrylate and the two peaks from the vinyl proton. Finally, the resulting PECMA was characterised by a methacrylation degree of 63.2 %, in accordance to other nethacrylated-bioinks reported in literature such as the most common Gelatin-Methacryloyl (GelMA) [34].

Gelation and water uptake properties. The gelation time tests were performed in bijou vial and exposed to UV light to determine the gelation time using a tube inversion method. The experiment was conducted under two different conditions: exposure to UV light and molarity of $CaCO_3$ solution as reported in Table 1. This gelation process involved evaluating the combination of both photo and ionic crosslinking mechanisms, that was achieved by introducing PBS solution (0.5 mL) containing the $CaCO_3$ at different molarity into the PECMA solutions (0.5 mL at 4 % w/v) before the UV exposure. The dual crosslinking approach in presence of higher content of $CaCO_3$ significantly accelerated the crosslinking process, reducing it to approximately 90 s (as evidenced by the inverted tests in Figure S1).

Furthermore, we examined the impact of the different molarity of the $CaCO_3$ ionic solutions and exposure to UV light on the water-uptake kinetics by immersing the hydrogels in a PBS solution for up to 48 h. The ionic crosslinking with the lowest molarity was not considered due the impossibility to crosslink properly the PECMA formulation. As shown in Table 1 no crosslinking was detected without UV light with 10 mM $CaCO_3$ solution while more than 30 min needed under UV exposure with the same crosslinking molarity. Fig. 3 shows that PECMA hydrogels exhibited remarkable hydrophilicity in all the conditions under consideration, with a rapid increase in water uptake within the first hour. Notably, PECMA hydrogels crosslinked with 40 mM $CaCO_3$ in both conditions with and without UV exposure displayed an exceptional water absorption capacity, reaching swelling equilibrium within just 2 h, indicating a high-water retention capability. In contrast, with highest molarity PECMA samples took as long as 8 h to reach the plateau. However, the exposure to UV showed that samples absorbed less water (853 ± 76 % with no UV vs. 612 ± 69 % with UV). Furthermore, the photocrosslinking to the ionic crosslinking led significantly to a reduced hydrophilicity, ranging from ~ 45 % to ~ 39 % for the samples crosslinked with 40 and 80 mM $CaCO_3$ respectively. According to these results, only the 80 mM $CaCO_3$ was used for the remaining physicochemical characterisation of the PECMA hydrogels.

By examining images depicting typical cross-sections of all the freeze-dried PECMA hydrogels, it becomes evident all samples exhibit a characteristic spongy three-dimensional morphology as shown in Fig. 4**A–D**. However, some discernible differences in the interior morphology of the analysed hydrogels were detected with and without the photocrosslinking. Indeed, without UV exposure the morphological structure of the samples was very inhomogeneous, characterised by larger pores and the presence of closed porosity (Fig. 4**A-B**), while with UV exposure the samples exhibited more open macropores, higher degree of interconnectivity and anisotropic porosity, forming a coherent network. This was further supported by the observed variations in the distribution of pore dimensions (Fig. 4**E**). In the case of absence of UV photocrosslinking, it was found that 28 % of the pores had a diameter less than 100 μm and ~ 50 % of pores with a diameter higher than 200 μm. In contrast, when exposed to UV, the samples had 64 % of pores with a diameter in the range between 100 and 200 μm, with the majority falling in the 150–200 μm range (35 %). A lower percentage of pores (18 %) with diameter higher than 200 μm was detected.

Table 1
Gelation time of PECMA hydrogels under the influence of different molarity of $CaCO_3$ and with the presence or absence of UV exposure.

$CaCO_3$ molarity (mM)	UV exposure (Yes/No)	Crosslinking time (min)
10	No	No crosslinking
10	Yes	35.5 ± 6.5
40	No	7.2 ± 1.5
40	Yes	4.5 ± 1.0
80	No	3.0 ± 0.5
80	Yes	1.5 ± 0.2

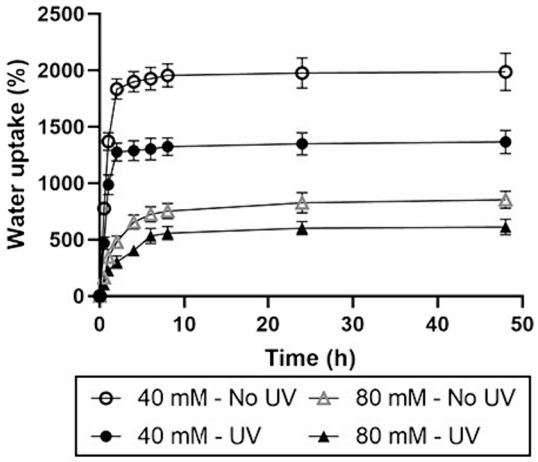

Fig. 3. Water uptake of PECMA hydrogels at different time points crosslinked with 40 and 80 mM $CaCO_3$ solution with and without exposure to UV light (n = 3).

Furthermore, to evaluate the additional mechanical properties, we utilised a rheometer to apply shear stress to the bioink systems (Fig. 5**A**), providing a valuable instrument for identifying the yield stress of materials. Specifically, the PECMA sample without UV crosslinking did not display a significant decrease in viscosity when flow initiated, unlike the UV crosslinked sample which exhibited a yield stress of 94.8 Pa. Additionally, Fig. 5**B** provided shear viscosity profiles for both samples, all of which exhibited shear-thinning behavior, indicated by a decrease in viscosity with increasing shear rate, where the effect of UV crosslinking on the PECMA sample was observed in higher viscosity over the low shear rate range compared to the uncrosslinked sample, which also demonstrated a Newtonian plateau below shear rates of ~ 0.8 s^{-1}. Also, Fig. 5**C** illustrates the distinctive relationship between the storage modulus (G') and the loss modulus (G'') as a function of oscillation stress for all the prepared hydrogels. Specifically, the frequency sweep test was employed to establish the connection between the testing frequency and the storage and loss moduli of a substance. It also offers insight into the viscoelastic characteristics and the material's condition by comparing the G' and G'' values across a range of frequencies [35]. The findings consistently indicated that the storage modulus (G') consistently exceeded the loss modulus (G'') across the entire frequency spectrum, and there was no observed point of intersection between the two curves. In each instance, G' consistently surpasses G'' (G'>G''), leading us to the inference that the sample is in a gel state [36]. Particularly, hydrogels under photocrosslinking showed higher G' values, reaching for example 2623.0 ± 97.7 kPa at 1 Hz, whereas for no UV exposure the samples recorded a G' of 1623.7 ± 89.2 kPa. This suggests that the addition of the UV crosslinked resulted in a more robust and cohesive intermolecular network, formed through polysaccharide interactions, as suggested by Bonino et al. for the development of methacrylated alginate-based hydrogels [37].

Furthermore, Fig. 5**D** shows the typical stress–strain (σ/ε) curve obtained from the compression tests for PECMA hydrogels crosslinked with 80 mM $CaCO_3$. From the linear part of the curve (0–10 % strain), a compressive elastic Young's modulus was calculated to be approximately 48.2 ± 5.6 kPa with UV exposure and 27.6 ± 3.1 kPa with no photocrosslinking, similar to the rheological frequency sweep tests. Beyond the linear region, there is a noticeable densification region, which is more pronounced in the PECMA sample suggested to both ionic and UV crosslinking. Interestingly, both sample types exhibited a strain

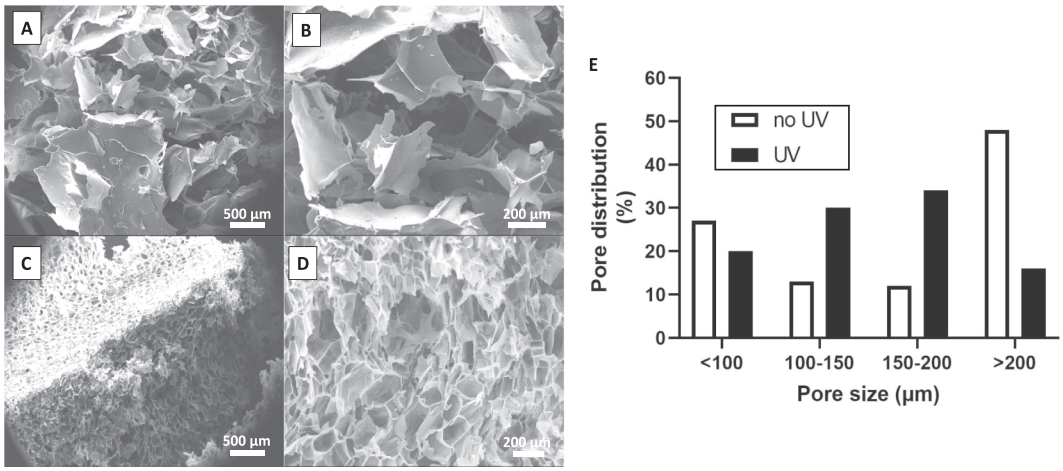

Fig. 4. SEM images displaying cross-sectional microstructures of the PECMA hydrogels without (**A**, **B**) and with (**C**, **D**) photocrosslinking under UV exposure; frequency of pore size within different diameter ranges (**E**).

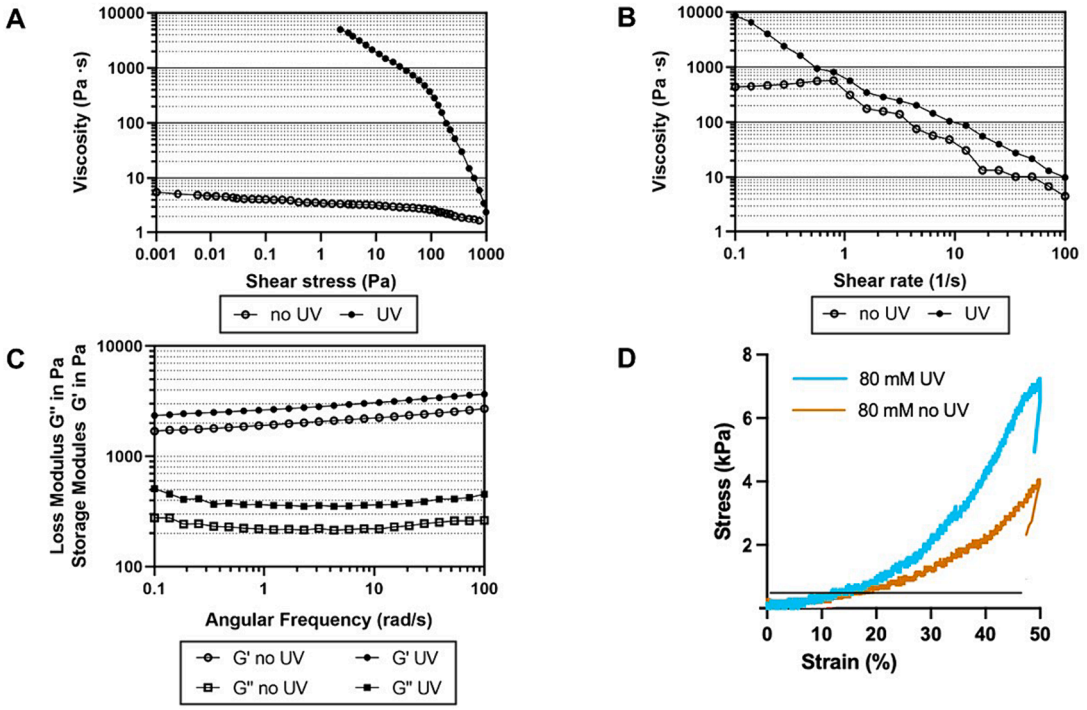

	UV		No UV	
	G' (Pa)	G'' (Pa)	G' (Pa)	G'' (Pa)
1 Hz	1623.7±89.2	214.9±39.9	2623.0±97.7	366.5±50.3
10 Hz	1901.3±102.6	226.7±30.1	3069.8±165.9	454.9±25.9

	UV	No UV
Young's modulus (Pa)	48.2±5.6	27.6±3.1
Strain at break (%)	49.1±0.3	49.5±0.4

Fig. 5. Rheological analyses for PECMA: (**A**) stress ramp test and (**B**) shear viscosity tests performed at 25 °C; (**C**) frequency sweep tests at 37 °C, displaying G' and G'' as angular frequency increases in the range of 0.1–20 %. (**D**) Representative stress–strain curves of the hydrogels with an without UV crosslinking under stati compression tests.

at break of ~ 50 %.

The metabolic activity of chondrocytes differentiated from human TERT immortalised bone marrow stromal cells was assessed using the PrestoBlue assay after 48 h of their culture with varying concentrations of extracted pectin to evaluate its compatibility (Fig. 6). It was observed an increase in metabolic activity with a decrease of the pectin concentration, corroborating the findings from the Live/Dead staining assay (Fig. 7). All samples containing extracted pectin promoted cell growth and rapid cell spreading, with a metabolic activity of 50 % detected at concentration range 1–20 mg/mL, and over 80 % with a concentration lower than 2.5 mg/mL. Furthermore, the viability of MSCs-C was assessed through a Live/Dead staining assay, as illustrated in Fig. 7. Lower concentrations demonstrated higher cell viability and an ability to facilitate cell attachment. MSCs-C exhibited a characteristic flattened and elongated morphology on all samples with extracted pectin, evenly spreading across the surface of the tissue culture plate. In

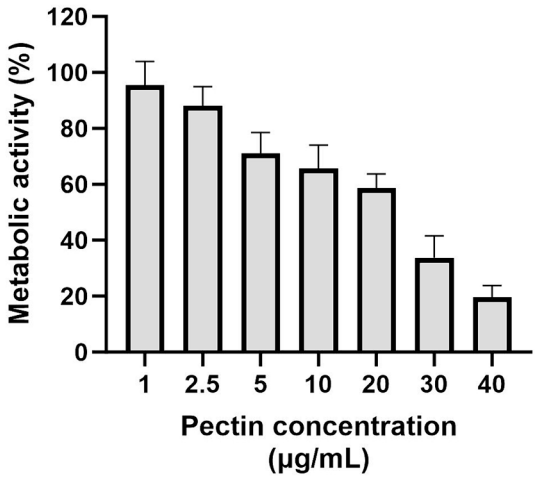

Fig. 6. The metabolic function of human TERT immortalised bone marrow stromal cells differentiated into chondrocytes assessed 48 h after seeding in the presence of various concentrations of extracted pectin, ranging from 1 to 40 mg/mL. The results are presented as the mean ± standard deviation after normalisation to the control group of cells that were seeded on tissue culture plates (TCPs).

contrast, higher concentrations seemed to affect cell behavior. Remarkably, at concentrations of 30 mg/mL and above, a reduced number of cells was observed with dead cells labelled in green. Immunostaining assays confirmed the previous results, with cells maintaining a spindle shape at low concentrations of extracted pectin. However, at higher concentrations, cells exhibited a rounded shape, cellular contraction, and smaller nuclei (Fig. 8). This could be attributed to the cytotoxic effects of pectin, as indicated by the low metabolic activity observed in the Presto Blue assay and the Live/Dead staining.

Finally, the ability to encapsulate cells in the PECMA-based bioink was tested and the cell metabolic activity was assessed at specific intervals: 48, 96 and 144 h (Fig. 9**A**). The PrestoBlue results indicated the existence of metabolically active cells with a decrease of the metabolic activity throughout the 6-day culture period (78554 ± 14476 at day 6 vs 157977 ± 15986 at day 2; $p < 0.05$). Fig. 9**B** shows the immunostaining images where the F-actin was labelled in green and the nuclei in blue. For this tests, the rhodamine phalloiding was not used due to the autofluorescence of the PECMA bioink in the red. The cells in all the culture period had a round-shape morphology, that was due to their encapsulation into the PECMA hydrogel, with a tendency to form agglomerate with the increase of the days of culture, as more evident at day 6 (Fig. 9**B-iii**). Finally, the bioprintability potential of the PECMA bioink has been demonstrated using the commercial Bio X Cellink bioprinter as shown in Figure S2 and Video S1 in the supplementary information.

4. Discussion

In this work, the cocoa pod husk, representing ~ 80 % of the fresh harvested fruit, was revalorised to extract pectin to be used in tissue engineering application. The optimised alkaline-based extraction process led to high PEC yield was ~ 20 %, exceeding the values reported in literature where the extracted pectin from cocoa pod husks using various extraction methods, primarily acidified water or enzymatic solutions, reached an extraction yield up to 14 % [3]. Furthermore, the sugar composition values were consistent with those reported for tomato pectin extracted under basic conditions and determined by PMP derivatisation method [26]. Specifically the galacturonic acid was found as the most abundant monoshoccaride while the measured content of the side regions indicated a branched and structurally heterogeneous PEC [38]. Also, the presence of glucose indicated the extraction of non-pectic polysaccharides such as hemicellulose and cellulose along with the pectin sample [7]. This characteristic can be induced by the extraction solvent (NaOH). Furthermore, the utilisation of alkaline solutions led to the formation of low methoxyl pectin (DE < 50 %) [39]. This consideration about the degree of esterification is vital when assessing the suitability of pectin for various biomedical applications, such as its utilisation as a bioink and hydrogel in tissue engineering and regenerative medicine. Specifically, low and high DE pectins require specific conditions for crosslinking. Pectin with a low DE is distinguished by a high number of free carboxyl groups, which exhibit a strong capacity to bind cations. The binding of divalent cations, like Ca^{2+} and Mg^{2+}, leads to the formation of junction zones between dimers of polyguluronate chains. These segments assume an “egg-box” structure, in which the cation binding to the carboxyl groups of two opposing pectin chains is stabilised by van der Waals interactions and hydrogen bonds [40]. Consequently, the extracted pectin becomes suitable for producing bioprinted constructs or in situ gelling systems. In our research, we employed $CaCO_3$ as the source of Ca^{2+} ions to facilitate the crosslinking of the hydrogels.

In our work, to confirm the successfull methacrylation process analysis using various chemical techniques were used. FTIR-ATR

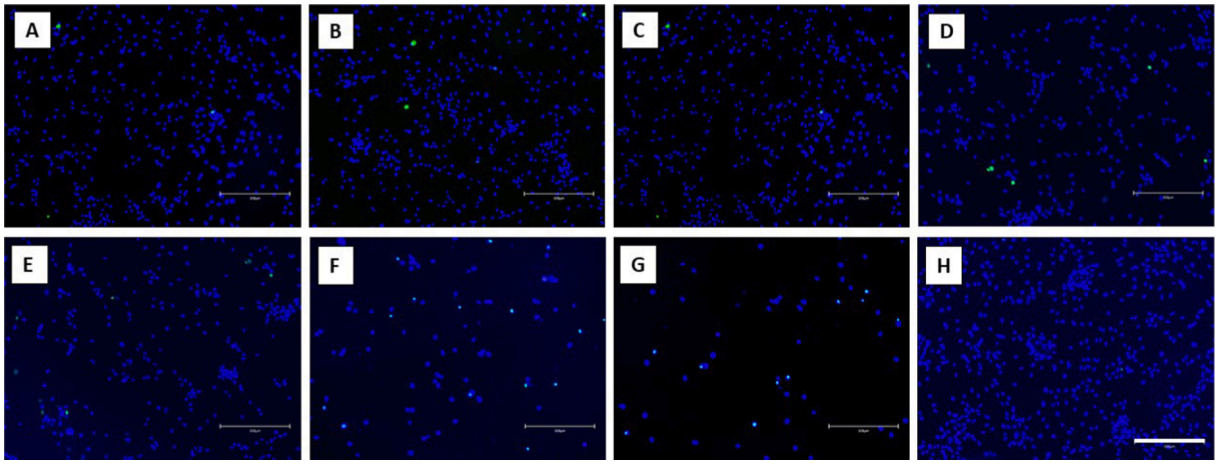

Fig. 7. Live/dead images of human TERT immortalised bone marrow stromal cells differentiated into chondrocytes (MSCs-C) captured after 48 h of seeding in the presence of varying concentrations: 1 mg/mL (**A**), 2.5 mg/mL (**B**), 5 mg/mL (**C**), 10 mg/mL (**D**), 20 mg/mL (**E**), 30 mg/mL (**F**) and 40 mg/mL (**G**) of the extracted pectin from cocoa biowaste. As control, MSC-Cs were cultured and differentiated into chondrocytes were seeded on the tissue culture plates (**H**). The scale bar is set at 300 µm.

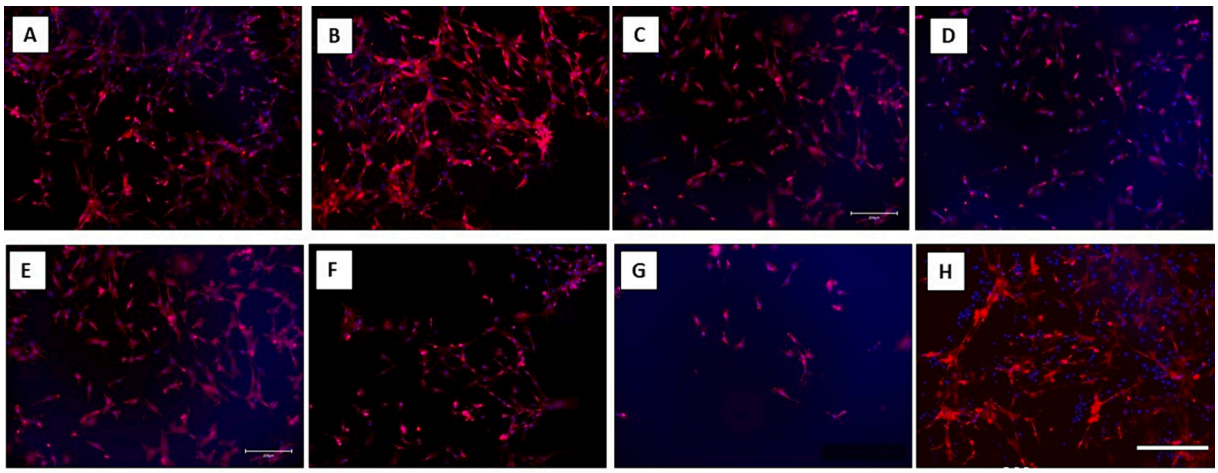

Fig. 8. Immunostaining images of human TERT immortalised bone marrow stromal cells differentiated into chondrocytes (MSCs-C) captured after 48 h of seeding in the presence of varying concentrations: 1 mg/mL (**A**), 2.5 mg/mL (**B**), 5 mg/mL (**C**), 10 mg/mL (**D**), 20 mg/mL (**E**), 30 mg/mL (**F**) and 40 mg/mL (**G**) of the extracted pectin from cocoa biowaste. As control, MSC-Cs were seeded on the tissue culture plates (**H**). The scale bar is set at 300 μm.

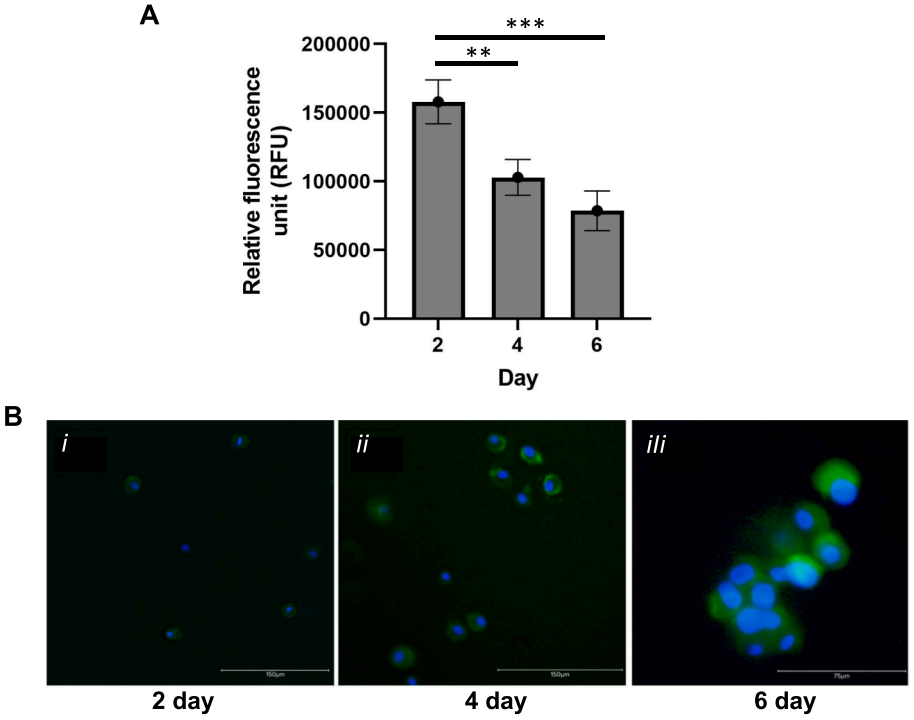

Fig. 9. The metabolic activity of MSCs-C cells encapsulated into the PECMA-based bioink assessed after 2, 4 and 6 days of incubation. The results are presented as the mean ± standard deviation. Tests were performed in triplicates. Statistics: ***$p < 0.001$, **$p < 0.01$ (**A**); Immunostaining images of MSCs-C cells encapsulated into the PECMA-based bioink assessed after 2, 4 and 6 days of incubation.

analysis was employed to investigate the chemical structure of pectin methacrylate and its biocompatibility. The reaction between pectin and methacrylate led to a significant increase in the presence of double bonds, including C = C and C = O groups, compared to pectin alone. This enhanced structural modification within the chemical bonds of pectin indicates that the incorporation of methacrylate moieties contributes to a substantial improvement in the overall rigidity of the material. The presence of numerous rotationally rigid double bonds restricts chain rotation, especially within the bulky side groups that enclose the compound, resulting in steric hindrance [33]. The presence of additional double bonds likely results in a stiffer material. From the FTIR-ATR spectra, the reaction between pectin and methacrylate resulted in a significant increase in the presence of double bonds, including C = C and C = O groups, when compared to pectin alone. This enhanced structural modification of the chemical bonds in pectin indicates that the incorporation of methacrylate moieties significantly enhances the overall rigidity of the material. The presence of numerous rotationally rigid double bonds restricts chain rotation, especially within the bulky side groups surrounding the compound, leading to steric hindrance. Furthermore, NMR spectroscopy confirmed the methacrylation of PEC by revealing the presence of methyl proton of methacrylate and the two peaks from the vinyl proton, which correspond to the mobility of methacrylate in the sample.

For hydrogel preparation, we selected a PECMA concentration of 2 % w/v. This choice was informed by the findings of Pereira et al., who observed that increasing the PEC polymer concentration from 1.5 % w/v

to 2.5 % w/v led to more pronounced aggregation of polymeric chains and enhanced physical and chemical crosslinking of the hydrogel formulation. This resulted in higher mechanical properties, which are crucial for the application of the developed constructs in regenerative medicine. Importantly, this adjustment did not negatively impact the cytocompatibility of the biomaterials [18]. While various divalent ions have potential as crosslinkers, our focus in this study was on the interaction between $CaCO_3$, as a source of Ca^{2+} ions, and the extracted pectin. Although there is extensive literature demonstrating the interaction of pectin with $CaCl_2$, primarily associated with its accelerated gelation speed and increased solubility, the rapid gelation of $CaCl_2$ can pose challenges in specific applications, such as 3D bioprinting, where precise control over gel swelling is essential [41]. Hence, $CaCO_3$, known for its established biocompatibility, has garnered attention. Research has shown that not only can the gelation time be controlled with $CaCO_3$, but also the extent of swelling can be managed. Due to these advantageous properties, we have chosen to explore the diverse potential that $CaCO_3$ offers combined with the UV polymerisation, that evidenced a gelation time ranging from 4 to 1.5 min in presence of 40 and 80 mM $CaCO_3$ under UV exposure. UV polimerisation is a photochemical reaction intended to yield more compact polymers and initiates the polymerisation of a monomer when triggered by a photoinitiator that absorbs UV radiation at a specific wavelength (365 nm in this experiment). This exposure converts the initiator into radicals, leading to the polymerisation of monomers in a structured composition [42,43]. LAP, a photoinitiator used in this context, initiates free radical chain polymerisation. Moreover, this photoinitiator is water-soluble, cytocompatible, and less cytotoxic than its predecessor, Irgacure 2959 [44]. Similar results have been reported by Scalzone et al [20], where the combination of photo- and ionic- crosslinking can be triggered by a reduction in temperature and the presence of divalent cations. They have introduced DMEM/F12 media, which contains various components, including $CaCl_2$, $MgSO_4$, Na_2HPO_4, KCl, and NaCl to gellan gum and gellan gum-manuka honey-based solutions. Employing this dual-crosslinking method significantly reduced the gelation time to approximately 3 min.

Moreover, for application in cartilage regeneration, as highlighted by Hannink et al [45], it si crucial to maintain a minimum pore size of approximately 100 μm to facilitate efficient transport of oxygen, nutrients, and waste materials. In our hydrogels prepared with UV crosslinking, the average pore size was found to be ~ 140 μm with high pores interconnectivity, signifying a favourable conditions for cell activities. On the other hand, when examining non-UV crosslinked hydrogels the average pore size was ~ 410 μm. Han et al. [46] outlined that the optimal range of porosity for cartilage regeneration lies between 100 and 200 μm and a porosity exceeding 400 μm is considered excessive, leading to elevated cell proliferation and compromised differentiation.

In order to investigate the mechanical characteristics of the hydrogels we created, we conducted compression testing and rheological analyses. First, to assess the viscoelastic behavior of the PECMA systems under static conditions, shear stress rheometry was conducted and plotting viscosity against shear stress allowed for the analysis of the viscosity at which material flow initiated, thereby enabling an approximation of its static viscosity. Only for the UV crosslinked PECMA sample, we were able to measure the yield stress (~98.4 Pa), that provided a valuable insights into its printability, because it indicated the threshold below which the material exhibited solid-like behavior rather than liquid-like behavior. Furthermore, both uncrosslinked and UV crosslinked PECMA exhibited a shear-thinning behavior, characterized by a reduction in viscosity with increasing shear rate. The trend in shear-thinning profiles for printable samples suggests the existence of a required viscosity window for successful ink extrusion while meeting initial screening conditions [30 47]. Moreover, in both scenarios with and without UV crosslinking, we successfully produced stable hydrogels with a Young's modulus (E) over 25 kPa, values aligned with what is commonly reported in the literature for the application of hydrogels in articular cartilage tissue engineering as observed in alginate-based hydrogels intended for differentiating mesenchymal stem cells in chondrocytes [48]. However, the results of our study highlighted the impact of utilising a dual crosslinking approach to enhance the material's Young's modulus. Specifically, the sample subjected to double crosslinking exhibited a higher Young's modulus compared to the other samples (48 kPa vs 28 kPa). Lin and colleagues have emphasised the significance of dual crosslinking in achieving a wider range of mechanical properties during hydrogel production[49]. Although the calculated Young's modulus of the prepared PECMA is lower than that of healthy human cartilage (ranging from 0.39 to 1.10 MPa calculated via AFM [50]), we found that double crosslinking can significantly improve the material's compressive stiffness. Furthermore, the culture of cells into the hydrogel will help the formation of new ECM and, consequently, expected to further enhance the Young's modulus. This trend was substantiated through rheological frequency sweep analyses from 0.1 to 100 Hz, covering the spectrum of frequencies associated with daily activities [51]. These tests indicated that the developed PECMA hydrogel was suitable for cartilage regeneration due to its superior viscoelastic properties, dominance in elasticity, and complex modulus. These characteristics enable the bioink to exhibit the characteristics of a soft gel, making it suitable for extrusion-based bioprinting [52]. To achieve precise structural accuracy in printed constructs, it becomes crucial to explore the connections between the structural attributes of hydrogel biomaterials and their flow properties. This underscores the significance of investigating these relationships through rheological studies [53]. Since G' was consistently higher than G'', the prepared bioink demonstrated increased stability. In terms of high-amplitude oscillatory shear, the formulated PECMA hydrogel can be categorised as type I, indicating shear-thinning behavior. As the strain increases, polymer chains untangle and align with the flow direction. This attribute is a key parameter in ensuring printability and enhancing mechanical rigidity, elastomeric characteristics, and physiological stability [54].

In our efforts to encapsulate chondrocytes within the PECMA hydrogel, the primary objective was to create a non-cytotoxic scaffold to allow cells to grow and produce their extracellular matrix, with the hydrogel serving as temporary support. Priorly to this, the extracted pectin from cocoa biowaste was assessed biologically using banked chondrocytes cells differentiated in our lab from Y201 clonal line derived from bone marrow, that showed good cytocompatibility with only adverse cellular behaviout at higher concentration (>30 mg/mL). These cells are known for proper development and differentiation, as it is more responsive to growth factors compared to mature chondrocytes [55]. This choice allowed for a time-efficient experiment since the range of cell differentiation required approximately two weeks of both cell culture and encapsulation [56]. Bone marrow-derived MSCs were preferred for their superior chondrogenic potential compared to MSCs from other tissues like adipose and muscle [57]. The Y201 strain was specifically chosen based on its previous use in various hydrogels, promoting chondrocyte development and cell spreading within a hydrogel [58]. This made it an ideal candidate for analysing PECMA's biological properties in cartilage regeneration compared to other MSC lines.

For the use bioink formulation, methacrylate, when combined with pectin, offers a promising attachment site for cartilage cells due to its simple gelling mechanism and cytocompatibility, enhancing cell survival as noted in reference [59]. To assess cell viability, we used the PrestoBlue assay, which is more sensitive and provides results that can be preserved for up to seven days without affecting performance [60]. The observed downward trend in metabolic activity over time is a natural process, reflecting the chondrocytes' transition toward maturity rather than cytotoxicity. Various factors, including the production of ECM and chondrogenesis, contribute to this decrease in metabolic activity. In the early stages of chondrogenesis, precursor cells of chondrocytes initiate the production of essential components of cartilage ECM, including proteoglycans, type II collagen, and aggrecan [56,61]. Therefore, the observed downward trend in metabolic activity is not a

result of cytotoxicity; rather, it reflects the natural progression of cells toward maturity. It has been well-established that chondrogenic differentiation of MSCs typically requires approximately two to three weeks under optimal culture conditions, a time frame consistent with our cell culture process that involves weeks of culturing and encapsulation, with regular media changes to provide necessary nutrients. Additionally, the culture medium includes a mixture of FBS containing TGF-β growth factor [62 63]. Moreover, the presence of glutamine in our DMEM medium serves various purposes, including the protection of chondrocyte survival, regulation of chondrogenic gene expression, and stimulation of ECM synthesis alongside chondrocyte proliferation. This contributes as an additional factor that aids in differentiating the MSCs-C cells in this experiment [64].

Moreover, the Live/Dead assay qualitatively confirmed the sustained viability of cells within the PECMA hydrogel for at least six days, indicating the cytocompatibility of the formulation. Additionally, the use of $CaCO_3$ as an ionic crosslinker did not affect cell condition, further demonstrating its compatibility [65,66]. F-Actin immunoassay results provided insights into cellular morphology and behavior, with the predominantly roundish shape of the F-actin cytoskeleton and with the formation of agglomerates with the increase of the culture time. This suggested optimal conditions for chondrogenic differentiation [67].

5. Conclusion

This research successfully revalorised cocoa pod husk, a major byproduct of cocoa processing, to extract pectin for potential use in biomedical field. The optimised alkaline-based extraction process yielded a high pectin yield of approximately 20 %, surpassing values reported in the literature for various extraction methods; the extracted pectin exhibited a branched and structurally heterogeneous nature, with a low methoxyl content, making it suitable for biomedical applications such as a versatile component for bioink formulations. Indeed, the methacrylated- pectin exhibited favorable properties for regenerative medicine, with a focus on cartilage regeneration. The choice of $CaCO_3$ as a source of Ca^{2+} ions, combined with UV polymersation using LAP as a photoinitiator, provided control over gelation time, swelling extent, rheological and mechanical properties essential for applications like 3D bioprinting. Furthermore, the encapsulation of chondrocytes within the PECMA hydrogels demonstrated high cytocompatibility, as evidenced by sustained cell viability and favorable cellular morphology and behavior. In summary, the revalorisation of cocoa pod husk into PECMA hydrogels showcased a promising approach for sustainable and functional biomaterials in tissue engineering and regenerative medicine. The study contributed valuable insights into the extraction, modification, and application of pectin from agricultural waste, paving the way for further exploration and development in the field of biomaterials for tissue engineering.

6. Declaration of Generative AI and AI-assisted technologies in the writing process

During the preparation of this work, the author(s) utilised ChatGPT 3.5 for proof-editing purposes. Following the use of this tool/service, the author(s) thoroughly reviewed and edited the content as necessary and take full responsibility for the content of the publication.

CRediT authorship contribution statement

Joel Girón-Hernández: Writing – review & editing, Writing – original draft, Supervision, Resources, Project administration, Investigation, Funding acquisition, Formal analysis, Data curation, Conceptualization. **Abraham Tombe:** . **Mufeeda Chemban Koyilot:** Writing – review & editing, Methodology, Formal analysis. **Karen T. Salas-Calderón:** Investigation, Formal analysis. **Alex Charlton:** Writing – review & editing, Writing – original draft, Methodology, Investigation, Formal analysis. **Corinne Wills:** Writing – review & editing, Writing – original draft, Methodology, Investigation, Formal analysis. **Piergiorgio Gentile:** Writing – original draft, Supervision, Resources, Project administration, Funding acquisition, Formal analysis, Conceptualization.

Declaration of competing interest

The authors declare that they have no known competing financial interests or personal relationships that could have appeared to influence the work reported in this paper.

Data availability

Data will be made available on request.

Acknowledgement

This work was supported by NERC Cross-disciplinary Research for Discovery Sciences (NE/X018229/1) and by Ministerio de Ciencia Tecnología e Innovación (project USCO VIPS-MC-3629).

Appendix A. Supplementary data

Supplementary data to this article can be found online at https://doi.org/10.1016/j.eurpolymj.2024.112967.

References

[1] Y.-C.-E. Li, Sustainable biomass materials for biomedical applications, ACS Biomater Sci. Eng. 5 (5) (2019) 2079–2092.
[2] J. Wang, W. Qian, Y. He, Y. Xiong, P. Song, R.-M. Wang, Reutilization of discarded biomass for preparing functional polymer materials, Waste Manag. 65 (2017) 11–21.
[3] Y.F. Barrios-Rodríguez, K.T. Salas-Calderón, D.A. Orozco-Blanco, P. Gentile, J. Girón-Hernández, Cocoa pod husk: a high-pectin source with applications in the food and biomedical fields, ChemBioEng Rev. 9 (5) (2022) 462–474.
[4] T.A. Toop, S. Ward, T. Oldfield, M. Hull, M.E. Kirby, M.K. Theodorou, AgroCycle–developing a circular economy in agriculture, Energy Procedia 123 (2017) 76–80.
[5] A.J. Garcia-Brand, M.A. Morales, A.S. Hozman, A.C. Ramirez, L.J. Cruz, A. Maranon, C. Muñoz-Camargo, J.C. Cruz, A. Porras, Bioactive poly (lactic acid)–cocoa bean shell composites for biomaterial formulation: Preparation and preliminary in vitro characterization, Polymers 13 (21) (2021) 3707.
[6] T.N. Tran, I.S. Bayer, J.A. Heredia-Guerrero, M. Frugone, M. Lagomarsino, F. Maggio, A. Athanassiou, Cocoa shell waste biofilaments for 3D printing applications, Macromol. Mater. Eng. 302 (11) (2017) 1700219.
[7] Y. Wandee, D. Uttapap, P. Mischnick, Yield and structural composition of pomelo peel pectins extracted under acidic and alkaline conditions, Food Hydrocoll. 87 (2019) 237–244.
[8] W.-L. Liang, J.-S. Liao, J.-R. Qi, W.-X. Jiang, X.-Q. Yang, Physicochemical characteristics and functional properties of high methoxyl pectin with different degree of esterification, Food Chem. 375 (2022) 131806.
[9] L. Wan, Z. Yang, R. Cai, S. Pan, F. Liu, S. Pan, Calcium-induced-gel properties for low methoxyl pectin in the presence of different sugar alcohols, Food Hydrocoll. 112 (2021) 106252.
[10] T. Agarwal, M. Costantini, T.K. Maiti, Extrusion 3D printing with pectin-based ink formulations: recent trends in tissue engineering and food manufacturing, Biomedical Engineering Advances 2 (2021) 100018.
[11] P.S. Gungor-Ozkerim, I. Inci, Y.S. Zhang, A. Khademhosseini, M.R. Dokmeci, Bioinks for 3D bioprinting: an overview, Biomater. Sci. 6 (5) (2018) 915–946.
[12] S. Ramesh, O.L. Harrysson, P.K. Rao, A. Tamayol, D.R. Cormier, Y. Zhang, I. V. Rivero, Extrusion bioprinting: recent progress, challenges, and future opportunities, Bioprinting 21 (2021) e00116.
[13] N.S. Bostancı, S. Büyüksungur, N. Hasirci, A. Tezcaner, Potential of pectin for biomedical applications: a comprehensive review, J. Biomater. Sci. Polym. Ed. 33 (14) (2022) 1866–1900.
[14] A.I. Cernencu, A. Lungu, I.-C. Stancu, A. Serafim, E. Heggset, K. Syverud, H. Iovu, Bioinspired 3D printable pectin-nanocellulose ink formulations, Carbohydr. Polym. 220 (2019) 12–21.
[15] A. Banks, X. Guo, J. Chen, S. Kumpaty, W. Zhang, Novel bioprinting method using a pectin based bioink, Technol. Health Care 25 (4) (2017) 651–655.
[16] H.-C. Chang, B. Jørgensen, L. Di Silvio, K. Gurzawska-Comis, 3D bioprinted pectin-based hydrogel as sustainable biomaterials for musculoskeletal tissue engineering, Sustain. Mater. Technol. 38 (2023) e00732.
[17] A. Lapomarda, G. Cerqueni, M.A. Geven, I. Chiesa, A. De Acutis, M. De Blasi, F. Montemurro, C. De Maria, M. Mattioli-Belmonte, G. Vozzi, Physicochemical

Characterization of pectin-gelatin biomaterial formulations for 3D bioprinting, Macromol. Biosci. 21 (9) (2021) 2100168.
[18] R.F. Pereira, A. Sousa, C.C. Barrias, P.J. Bártolo, P.L. Granja, A single-component hydrogel bioink for bioprinting of bioengineered 3D constructs for dermal tissue engineering, Mater. Horiz. 5 (6) (2018) 1100–1111.
[19] R.F. Pereira, B.N. Lourenço, P.J. Bártolo, P.L. Granja, Bioprinting a multifunctional bioink to engineer clickable 3D cellular niches with tunable matrix microenvironmental cues, Adv. Healthc. Mater. 10 (2) (2021) 2001176.
[20] A. Scalzone, G. Cerqueni, M.A. Bonifacio, M. Pistillo, S. Cometa, M.M. Belmonte, X. N. Wang, K. Dalgarno, A.M. Ferreira, E. De Giglio, Valuable effect of manuka honey in increasing the printability and chondrogenic potential of a naturally derived bioink, Materials Today Bio 14 (2022) 100287.
[21] J. Girón, L. Gil-Sánchez, E. García-Breijo, M.J. Pagán, J.M. Barat, R. Grau, Development of potentiometric equipment for the identification of altered dry-cured hams: a preliminary study, Meat Sci. 106 (2015) 1–5.
[22] J. Cui, W. Ren, C. Zhao, W. Gao, G. Tian, Y. Bao, Y. Lian, J. Zheng, The structure–property relationships of acid-and alkali-extracted grapefruit peel pectins, Carbohydr. Polym. 229 (2020) 115524.
[23] J. Girón-Hernández, M. Pazmino, Y.F. Barrios-Rodríguez, C.T. Turo, C. Wills, F. Cucinotta, M. Benlloch-Tinoco, P. Gentile, Exploring the effect of utilising organic acid solutions in ultrasound-assisted extraction of pectin from apple pomace, and its potential for biomedical purposes, Heliyon 9 (7) (2023).
[24] L. Zhou, G. Tan, Y. Tan, H. Wang, J. Liao, C. Ning, Biomimetic mineralization of anionic gelatin hydrogels: effect of degree of methacrylation, RSC Adv. 4 (42) (2014) 21997–22008.
[25] J. Dai, Y. Wu, S.-W. Chen, S. Zhu, H.-P. Yin, M. Wang, J. Tang, Sugar compositional determination of polysaccharides from Dunaliella salina by modified RP-HPLC method of precolumn derivatization with 1-phenyl-3-methyl-5-pyrazolone, Carbohydr. Polym. 82 (3) (2010) 629–635.
[26] R. Slimestad, V. Holm, H. Barsett, Sample Preparation and analysis of tomato pectin Monomers, Chromatographia 82 (2019) 975–981.
[27] S.H. Jong, N. Abdullah, N. Muhammad, Effect of acid type and concentration on the yield, purity, and esterification degree of pectin extracted from durian rinds, results, Engineering (2023) 100974.
[28] A. Chatjigakis, C. Pappas, N. Proxenia, O. Kalantzi, P. Rodis, M. Polissiou, FT-IR spectroscopic determination of the degree of esterification of cell wall pectins from stored peaches and correlation to textural changes, Carbohydr. Polym. 37 (4) (1998) 395–408.
[29] M. Brittberg, A. Lindahl, A. Nilsson, C. Ohlsson, O. Isaksson, L. Peterson, Treatment of deep cartilage defects in the knee with autologous chondrocyte transplantation, N. Engl. J. Med. 331 (14) (1994) 889–895.
[30] N. Paxton, W. Smolan, T. Böck, F. Melchels, J. Groll, T. Jungst, Proposal to assess printability of bioinks for extrusion-based bioprinting and evaluation of rheological properties governing bioprintability, Biofabrication 9 (4) (2017) 044107.
[31] A. Scalzone, X.N. Wang, K. Dalgarno, A.M. Ferreira, P. Gentile, A chondrosphere-based scaffold free approach to manufacture an in vitro articular cartilage model, Tissue Eng. A 28 (1–2) (2022) 84–93.
[32] J.-H. Wang, C.-W. Tsai, N.-Y. Tsai, C.-Y. Chiang, R.-S. Lin, R.F. Pereira, Y.-C.-E. Li, An injectable, dual crosslinkable hybrid pectin methacrylate (PECMA)/gelatin methacryloyl (GelMA) hydrogel for skin hemostasis applications, Int. J. Biol. Macromol. 185 (2021) 441–450.
[33] M. Mehrali, A. Thakur, F.B. Kadumudi, M.K. Pierchala, J.A.V. Cordova, M.-A. Shahbazi, M. Mehrali, C.P. Pennisi, G. Orive, A.K. Gaharwar, Pectin methacrylate (PEMA) and gelatin-based hydrogels for cell delivery: converting waste materials into biomaterials, ACS Appl. Mater. Interfaces 11 (13) (2019) 12283–12297.
[34] Z. Wang, Z. Tian, F. Menard, K. Kim, Comparative study of gelatin methacrylate hydrogels from different sources for biofabrication applications, Biofabrication 9 (4) (2017) 044101.
[35] G. Stojkov, Z. Niyazov, F. Picchioni, R.K. Bose, Relationship between structure and rheology of hydrogels for various applications, Gels 7 (4) (2021) 255.
[36] T. Gao, G.J. Gillispie, J.S. Copus, A.K. Pr, Y.-J. Seol, A. Atala, J.J. Yoo, S.J. Lee, Optimization of gelatin–alginate composite bioink printability using rheological parameters: a systematic approach, Biofabrication 10 (3) (2018) 034106.
[37] C.A. Bonino, J.E. Samorezov, O. Jeon, E. Alsberg, S.A. Khan, Real-time in situ rheology of alginate hydrogel photocrosslinking, Soft Matter 7 (24) (2011) 11510–11517.
[38] E.D. Ngouémazong, S. Christiaens, A. Shpigelman, A. Van Loey, M. Hendrickx, The emulsifying and emulsion-stabilizing properties of pectin: a review, Compr. Rev. Food Sci. Food Saf. 14 (6) (2015) 705–718.
[39] M. Axelos, J. Thibault, The chemistry of low-methoxyl pectin gelation, The Chemistry and Technology of Pectin 6 (1991) 109.
[40] I. Popescu, M. Lupei, M. Constantin, G. Voicu, M. Calin, A.I. Prisacaru, G. Fundueanu, Double cross-linked pectin beads stable in physiological environment as potential support for biomedical applications, J. Polym. Res. 28 (2021) 1–16.
[41] S. Houben, L.M. Pitet, Ionic crosslinking strategies for poly (acrylamide)/alginate hybrid hydrogels, React. Funct. Polym. 191 (2023) 105676.
[42] M. Worzakowska, UV polymerization of methacrylates—preparation and properties of novel copolymers, Polymers 13 (10) (2021) 1659.
[43] G. Choi, H.J. Cha, Recent advances in the development of nature-derived photocrosslinkable biomaterials for 3D printing in tissue engineering, Biomaterials Research 23 (1) (2019) 1–7.
[44] A. Nguyen, P. Goering, R. Elespuru, S. Das, R. Narayan, The photoinitiator lithium phenyl (2, 4, 6-Trimethylbenzoyl) phosphinate with exposure to 405 nm light is cytotoxic to mammalian cells but not mutagenic in bacterial reverse mutation assays, Polymers 12 (7) (2020) 1489.
[45] G. Hannink, J.C. Arts, Bioresorbability, porosity and mechanical strength of bone substitutes: what is optimal for bone regeneration? Injury 42 (2011) S22–S25.
[46] Y. Han, M. Lian, Q. Wu, Z. Qiao, B. Sun, K. Dai, Effect of pore size on cell behavior using melt electrowritten scaffolds, Front. Bioeng. Biotechnol. 9 (2021) 629270.
[47] A.F. Bonatti, I. Chiesa, G. Vozzi, C. De Maria, Open-source CAD-CAM simulator of the extrusion-based bioprinting process, Bioprinting 24 (2021) e00172.
[48] F.E. Freeman, D.J. Kelly, Tuning alginate bioink stiffness and composition for controlled growth factor delivery and to spatially direct MSC fate within bioprinted tissues, Sci. Rep. 7 (1) (2017) 17042.
[49] P. Lin, T. Zhang, X. Wang, B. Yu, F. Zhou, Freezing molecular orientation under stretch for high mechanical strength but anisotropic hydrogels, Small 12 (32) (2016) 4386–4392.
[50] M. Wang, Z. Peng, J.A. Watson, G.S. Watson, B.N. Morris, B. Rayner, Atomic Force Microscopy Investigation on Young's Modulus of Cartilage for Osteoarthritis Study, Engineering Asset Management and Infrastructure Sustainability: Proceedings of the 5th World Congress on Engineering Asset Management (WCEAM 2010), Springer, 2012, pp. 1019-1025.
[51] S. Perni, P. Prokopovich, Rheometer enabled study of cartilage frequency-dependent properties, Sci. Rep. 10 (1) (2020) 20696.
[52] S. Mudavath, S. Arvapalli, A review on recent advances in 3D bioprinting, international journal of Pharmaceutical and bio, Med. Sci. 2 (11) (2022) 484–493.
[53] A. Bandyopadhyay, B.B. Mandal, N. Bhardwaj, 3D bioprinting of photo-crosslinkable silk methacrylate (SilMA)-polyethylene glycol diacrylate (PEGDA) bioink for cartilage tissue engineering, J. Biomed. Mater. Res. A 110 (4) (2022) 884–898.
[54] A. Thakur, M.K. Jaiswal, C.W. Peak, J.K. Carrow, J. Gentry, A. Dolatshahi-Pirouz, A.K. Gaharwar, Injectable shear-thinning nanoengineered hydrogels for stem cell delivery, Nanoscale 8 (24) (2016) 12362–12372.
[55] P. Kopesky, H.-Y. Lee, E. Vanderploeg, J. Kisiday, D. Frisbie, A. Plaas, C. Ortiz, A. Grodzinsky, Adult equine bone marrow stromal cells produce a cartilage-like ECM mechanically superior to animal-matched adult chondrocytes, Matrix Biol. 29 (5) (2010) 427–438.
[56] L.A. Solchaga, K.J. Penick, J.F. Welter, Chondrogenic differentiation of bone marrow-derived mesenchymal stem cells: tips and tricks, Mesenchymal Stem Cell Assays and Applications (2011) 253–278.
[57] H. Koga, T. Muneta, T. Nagase, A. Nimura, Y.-J. Ju, T. Mochizuki, I. Sekiya, Comparison of mesenchymal tissues-derived stem cells for in vivo chondrogenesis: suitable conditions for cell therapy of cartilage defects in rabbit, Cell Tissue Res. 333 (2008) 207–215.
[58] A. Galarza Torre, J.E. Shaw, A. Wood, H.T. Gilbert, O. Dobre, P. Genever, K. Brennan, S.M. Richardson, J. Swift, An immortalised mesenchymal stem cell line maintains mechano-responsive behaviour and can be used as a reporter of substrate stiffness, Sci. Rep. 8 (1) (2018) 8981.
[59] F. Munarin, M.C. Tanzi, P. Petrini, Advances in biomedical applications of pectin gels, Int. J. Biol. Macromol. 51 (4) (2012) 681–689.
[60] M. Xu, D.J. McCanna, J.G. Sivak, Use of the viability reagent PrestoBlue in comparison with alamarBlue and MTT to assess the viability of human corneal epithelial cells, J. Pharmacol. Toxicol. Methods 71 (2015) 1–7.
[61] S. Ammendola, A.S. d'Abusco, Oxidative stress, senescence and Mediterranean diet effects on osteoarthritis, Aging, Elsevier (2020) 73–81.
[62] T. Oida, H.L. Weiner, Depletion of TGF-β from fetal bovine serum, J. Immunol. Methods 362 (1–2) (2010) 195–198.
[63] H. Chen, X.-N. Tan, S. Hu, R.-Q. Liu, L.-H. Peng, Y.-M. Li, P. Wu, Molecular mechanisms of chondrocyte proliferation and differentiation, Front. Cell Dev. Biol. 9 (2021) 664168.
[64] S. Stegen, G. Rinaldi, S. Loopmans, I. Stockmans, K. Moermans, B. Thienpont, S.-M. Fendt, P. Carmeliet, G. Carmeliet, Glutamine metabolism controls chondrocyte identity and function, Dev. Cell 53 (5) (2020) 530–544, e8.
[65] M. Costantini, J. Idaszek, K. Szöke, J. Jaroszewicz, M. Dentini, A. Barbetta, J. E. Brinchmann, W. Święszkowski, 3D bioprinting of BM-MSCs-loaded ECM biomimetic hydrogels for in vitro neocartilage formation, Biofabrication 8 (3) (2016) 035002.
[66] P. Xu, F. Jiang, H. Zhang, R. Yin, L. Cen, W. Zhang, Calcium carbonate/gelatin methacrylate microspheres for 3D cell culture in bone tissue engineering, Tissue Eng. Part C Methods 26 (8) (2020) 418–432.
[67] L. Gao, R. McBeath, C.S. Chen, Stem cell shape regulates a chondrogenic versus myogenic fate through Rac1 and N-cadherin, Stem Cells 28 (3) (2010) 564–572.